Cation exchange synthesis and optoelectronic properties of type II CdTe–$Cu_{2-x}Te$ nano-heterostructures†

Ilka Kriegel,‡*[ab] Andreas Wisnet,[db] Ajay Ram Srimath Kandada,[e] Francesco Scotognella,[c] Francesco Tassone,[e] Christina Scheu,[db] Hui Zhang,[f] Alexander O. Govorov,[f] Jessica Rodr guez-Fernández*[ab] and Jochen Feldmann[ab]

Rod-shaped CdTe–$Cu_{2-x}Te$ nano-heterostructures with tunable dimensions of both sub-units and a type II band alignment were prepared by Cd^{2+}/Cu^{+} cation exchange. The light absorption properties of the heterostructures are dominated by the excitonic and plasmonic contributions arising, respectively, from the CdTe and the $Cu_{2-x}Te$ sub-units. These results were confirmed over a wide range of sub-unit length fractions through optical modelling based on the discrete dipole approximation (DDA). Although assuming electronically independent sub-units, our modelling results indicate a negligible ground state interaction between the CdTe exciton and the $Cu_{2-x}Te$ plasmon. This lack of interaction may be due to the low spectral overlap between exciton and plasmon, but also to localization effects in the vacancy-doped sub-unit. The electronic interaction between both sub-units was evaluated with pump-probe spectroscopy by assessing the relaxation dynamics of the excitonic transition. In particular, the CdTe exciton decays faster in the presence of the $Cu_{2-x}Te$ sub-unit, and the decay gets faster with increasing its length. This points towards an increased probability of Auger mediated recombination due to the high carrier density in the $Cu_{2-x}Te$ sub-unit. This indication is supported through length-fraction dependent band structure calculations, which indicate a significant leakage of the CdTe electron wavefunction into the $Cu_{2-x}Te$ sub-unit that increases along with the shortening of the CdTe sub-unit, thus enhancing the probability of Auger recombination. Therefore, for the application of type II chalcogenide–chalcogenide heterostructures based on Cu and Cd for photoenergy conversion, a shorter Cu-based sub-unit may be advantageous, and the suppression of high carrier density within this sub-unit is of high importance.

Received 16th October 2013
Accepted 28th November 2013

Introduction

Synthesis strategies to design colloidal heterostructures that combine materials with different functionalities have gained increasing attention in recent years.[1–3] The combination of a semiconductor and a metal in one nano-heterostructure is of particular interest because nano-heterostructures with the distinctive excitonic and plasmonic properties of both counterparts can be obtained.[3,4] Such a combination of very different materials in one nanostructure may result in new physical properties.[1,2,4–9] For instance, metal–semiconductor hybrids have been demonstrated to trigger redox reactions when used for photocatalytic fuel generation.[2,10–16] Another interesting aspect of the metal–semiconductor nanostructures is in the exciton–plasmon interaction and in the resulting effect of Fano interference,[17–20] which can be used to tailor the optical transmission of a nanomaterial. Semiconductor–semiconductor nano-heterostructures are of fundamental interest as well. A control over the size, shape or interface area enables a careful engineering of the relative band alignments of both semiconductors and thus enables a tight control over the physical

[a]*Photonics and Optoelectronics Group, Department of Physics and CeNS, Ludwig-Maximilians-Universität München, Munich, Germany. E-mail: ilka.kriegel@polimi.it; jessica.rodriguez@lmu.de; Web: http://www.phog.physik.uni-muenchen.de/*
[b]*Nanosystems Initiative Munich (NIM), Munich, Germany*
[c]*Dipartimento di Fisica, Politecnico di Milano, piazza Leonardo da Vinci 32, 20133 Milano, Italy*
[d]*Department of Chemistry and CeNS, Ludwig-Maximilians-Universität München, Munich, Germany*
[e]*CNST of IIT@POLIMI, Via Pascoli 70/3, 20133 Milano, Italy*
[f]*Department of Physics and Astronomy, Ohio University, Athens, Ohio 45701, USA*

† Electronic supplementary information (ESI) available: Evidence of $Cu_{2-x}Te$ sub-unit degradation upon electron beam exposure (Fig. S1); experimental absorption spectra of CdTe–$Cu_{2-x}Te$ heterostructures with different sub-unit fractions, focussing on the region of the CdTe exciton (Fig. S2) and on the region of the $Cu_{2-x}Te$ plasmon resonance (Fig. S3); photoluminescence spectra of CdTe–$Cu_{2-x}Te$ NRs prepared by cation exchange *via* addition of increasing amounts of Cu^{+} (Fig. S4). See DOI: 10.1039/c3tc32049a

‡ Current address: Dipartimento di Fisica, Politecnico di Milano, piazza Leonardo da Vinci 32, 20133 Milano, Italy.

and optical properties of the hybrid nanostructures.[21–34] For instance, in type I core/shell heterostructures the particular band alignment of both semiconductors results in the confinement of the charges in the core material.[31,33,35] In contrast, in heterostructures with a type II staggered band alignment the charges may spatially separate after photoexcitation,[36,37] and thus this makes them interesting for photovoltaic and photocatalytic applications. In either case a fast charge separation and a slow recombination of charges are key requirements.[33,37] Type II heterostructures consisting of cadmium- and copper-based chalcogenides as semiconductor materials have been highlighted as good candidates for photoenergy conversion and special attention has been given to anisotropic nano-heterostructures resulting from the combination of CdS and $Cu_{2-x}S$.[37–39]

One strategy to obtain semiconductor–semiconductor nano-heterostructures consists of exploiting the existence of a highly reactive surface of a nanocrystal (NC) made of a semiconductor A to favor the epitaxial growth of a semiconductor B.[40,41] Another approach to fabricate semiconductor–semiconductor nano-heterostructures with given shapes and composition, and a well-defined hetero-interface, is given by cation exchange.[42–50] During this process the cations in an ionic solid can be replaced by other cations.[42] In most cases, when performed on anisotropic nanocrystals, cation exchange occurs preferentially from one direction.[38,42,44–46,48] In this way it is possible to create nano-heterostructures made out of two dissimilar semiconductors and to exert a certain control over the size of both sub-units by controlling the amount of the exchanging cation added.[38,42–49] An additional benefit of this approach is that the initial shape of the NC is preserved during the ion exchange process and sharp hetero-interfaces are obtained.[42,44,47,48,51] Thus, cation exchange is a fast and efficient, single-step approach, performed at room temperature, and in a straightforward manner, yet with a high control over the growth of the respective sub-units.[42]

In this work we have selected CdTe and $Cu_{2-x}Te$ as the semiconductors of choice for the preparation of type II nano-heterostructures *via* cation exchange. CdTe as a typical II-VI semiconductor exhibits strong excitonic properties at the nanoscale when the NC size lies in the region of the exciton Bohr radius.[52–56] This is due to the local confinement of the electron–hole pair to barriers governed by the NC dimensions.[56] On the other hand $Cu_{2-x}Te$, in analogy to other copper chalcogenides, belongs to the class of vacancy-doped semiconductors.[57–59] This special characteristic originates from vacancies in the structure that ultimately lead to a highly increased carrier (hole) density on the order of 10^{21} cm^{-3}, and therefore to localized surface plasmon resonances in the near infrared (NIR) region.[57–67] Here we will show how the progressive exchange of Cd^{2+} in the initial CdTe nanorods (NRs) by Cu^{+} ions leads to well-defined CdTe–$Cu_{2-x}Te$ nano-heterostructures. By performing a length-fraction dependent investigation, we addressed the role of the excitonic and plasmonic contribution to the optical response of the entire system, while taking into account the type II band alignment of the semiconductor–semiconductor nano-heterostructure and its highly increased carrier density. All such factors are strongly relevant for any physical interpretation and in particular with respect to a possible application of this material system in photoenergy conversion applications.

Experimental

Synthesis of CdTe NRs

We synthesized CdTe NRs according to the work of Shieh *et al.*[68] First, the Cd precursor was prepared by degassing a mixture of 0.114 g CdO, 0.43 g TDPA (*n*-tetradecylphosphonic acid) and 7 g of TOPO (trioctylphosphine oxide) at 120 °C for one hour. The mixture was heated to 350 °C under nitrogen until the solution turned clear. The Te precursor solution was prepared by dissolving 0.255 g Te in 10 mL TOP (trioctylphosphine [TOP] = 0.2 M) under vigorous stirring at 150 °C for *ca.* 1 h in a N_2 filled glovebox. The temperature of the Cd precursor solution was lowered to 290 °C for injection of 0.5 mL of the Te–TOP precursor. After injection the temperature dropped to 280 °C. Thereafter the temperature was increased to 290 °C, followed by the subsequent injection of 0.5 mL Te–TOP solutions every 2 min until a total of 4 mL were injected. After reaction the solution was allowed to cool down to 70 °C when 15 mL of anhydrous toluene were added to the reaction mixture with the aid of a syringe. The resulting CdTe NR solution was transferred to a glovebox for handling. The sample was precipitated 2× with 30 mL of anhydrous ethanol followed by centrifugation (6000 rpm, 5 min). The NRs were finally redispersed in 10 mL of anhydrous toluene.

Preparation of CdTe–$Cu_{2-x}Te$ nano-heterostructures *via* cation exchange

We used tetrakis(acetonitrile)copper(I) hexafluorophosphate ($[(CH_3CN)_4Cu]PF_6$, Sigma Aldrich) as the Cu^{+} source. All steps were performed in a N_2 filled glovebox and anhydrous solvents were used in all preparation procedures. Oleylamine (OAm) was acquired from Sigma Aldrich and degassed for 24 h before use. To perform the ion exchange reaction we first determined the concentration of a known CdTe NR dilution by following standard procedures as described in ref. 69 for spherical NCs. This provided an upper limit to determine the amount of Cu^{+} to be added. For ion exchange, the $[(CH_3CN)_4Cu]PF_6$ is first dissolved in methanol to a concentration of 4 mg mL^{-1}. In a typical exchange reaction, 3 mL of methanol, 1.5 mL of toluene and an exact amount of Cu^{+} solution (typically 25, 50, 75, or 100 μL) in methanol are mixed and stirred. Then 30 μL of a CdTe NR stock dispersion ([CdTe] ∼ 0.06 mmol L^{-1}) are added. Complete exchange is achieved by adding a 10× stoichiometric excess of Cu^{+} with respect to the amount of Cd^{2+}. To compensate for the loss of ligands upon exchange of Cd^{2+} by Cu^{+} surface atoms and to stabilize the NRs after redispersion, 100 μL of oleylamine are added to the initial colloidal solution. Once the reaction is completed the colloidal dispersion is transferred to centrifugation tubes and the NRs are centrifuged at 6000 rpm for 5 min. The supernatant is discarded and the dark brown precipitate

containing the ion exchanged NRs is redispersed in 1 mL of toluene or tetrachloroethylene (TCE) for further experiments.

Characterization

Optical characterization. UV-vis-NIR extinction spectra of all NCs were measured in 1 cm path length NIR quartz cuvettes using a Cary 5000 UV-vis-NIR spectrophotometer. All sample preparation procedures were carried out in a N_2 filled glovebox. Anhydrous solvents were used in all cases. The NRs were redispersed in tetrachloroethylene for measurements in the NIR.

Structural characterization. Wide-angle powder X-ray diffraction (XRD) patterns were collected using a Bruker D8 diffractometer with a Cu Kα X-ray source operating at 40 kV and 40 mA and a Vantec 2000 area detector. The assignment of crystalline phases was based on the reference files in the Powder Diffraction File (PDF-2) database from International Center for Diffraction Data (ICDD). For XRD characterization the NRs were precipitated, redispersed in a very low amount of toluene and drop-casted onto a glass cover slip. The cover slip was placed on a hotplate at ~100 °C to allow for fast solvent evaporation.

Electron microscopy characterization. Transmission electron microscopy (TEM), scanning transmission electron microscopy (STEM) and energy dispersive X-ray spectroscopy (EDX) measurements were performed on an FEI Titan 80-300 S/TEM equipped with an EDAX EDX detector. TEM grids were prepared by drop-casting 5 μL of the corresponding NR sample in toluene onto a carbon-coated Cu TEM grid. The remaining solvent was removed with a filter paper.

Transient absorption measurements. For transient absorption spectroscopy we used a system based on a Ti-Sapphire chirp pulse amplified source, with a maximum output energy of about 800 μJ, repetition rate of 1 kHz, central wavelength of 780 nm and pulse duration of about 180 fs. Excitation pulses at 670 nm were generated by non-collinear optical parametric amplification in β-barium borate (BBO), with pulse duration around 100 fs.[70] Pump pulses were focused in a 200 μm diameter spot. Probing was achieved in the visible region by using white light generated in a thin sapphire plate. Chirp-free transient transmission spectra were collected by using a fast optical multichannel analyzer (OMA) with dechirping algorithm. The measured quantity is the normalized transmission change, $\Delta T/T$. The excitation energy was kept at ~20 nJ, in order to prevent saturation of the optical transitions. All measurements were performed at room temperature with the NRs dispersed in toluene.

Effective mass calculations. We used the finite element method to solve the Schrödinger equation for the electron envelope function resulting from the effective mass approximation.[71] We considered bulk effective masses for electrons in CdTe and $Cu_{2-x}Te$ of $0.0963m_0$ and $0.0476m_0$, respectively. The effective mass of the latter was estimated according to the $k\cdot p$ theory from a band gap energy (E_g) of 1.04 eV. We used a conduction band offset (ΔE_c) between CdTe and $Cu_{2-x}Te$ of 0.34 eV, as determined *via* XPS and UPS measurements on bulk $Cu_{2-x}Te$ layers deposited on bulk CdTe films (E_g = 1.49 eV).[72] For details on the CdTe–$Cu_{2-x}Te$ band alignment, see the schematic representation in Fig. 4d.

Results and discussion

We synthesized CdTe NRs as a starting material, following a standard procedure for CdTe NR synthesis.[68] In short, a Te–TOP precursor solution is injected into a Cd precursor solution prepared in TDPA and TOPO at 290 °C with subsequent injections every 2 minutes (see Experimental section for details). A typical TEM image of the obtained CdTe NRs (Fig. 1a) shows the formation of uniform NRs with an average width of 5 nm and an average length of 21 nm. To prepare the CdTe–$Cu_{2-x}Te$ nanoheterostructures, an excess of Cu^+ ions in solution is added to the CdTe NRs to trigger the cation exchange reaction. Typically, 3 mL of methanol, 1.5 mL of toluene and an exact amount (25, 50, 75, or 100 μL) of the Cu^+ stock solution ($[(CH_3CN)_4Cu]PF_6$ in methanol, 4 mg mL^{-1}) are first stirred in a glovebox. Thereafter 30 μL of the CdTe NRs in toluene ([CdTe] ~ 0.06 mmol L^{-1}) are added to the mixture and stirred for 1–2 additional min. This way, depending on the amount of Cu^+ precursor added, we obtain rod-shaped heterostructures with CdTe and $Cu_{2-x}Te$ sub-units of varying sizes. By adding a 10× stoichiometric excess of the Cu^+ precursor with respect to the amount of Cd^{2+}, complete ion exchange occurs (*i.e.*, $Cu_{2-x}Te$ NR formation).[57] Note that to avoid NR destabilization arising from the loss of ligands upon Cd^{2+}/Cu^+ cation exchange, oleylamine is added to the starting CdTe NRs. In any case, regardless of partial (Fig. 1b) or complete (Fig. 1c) cation exchange, the initial nanorod shape and size (Fig. 1a) is preserved.

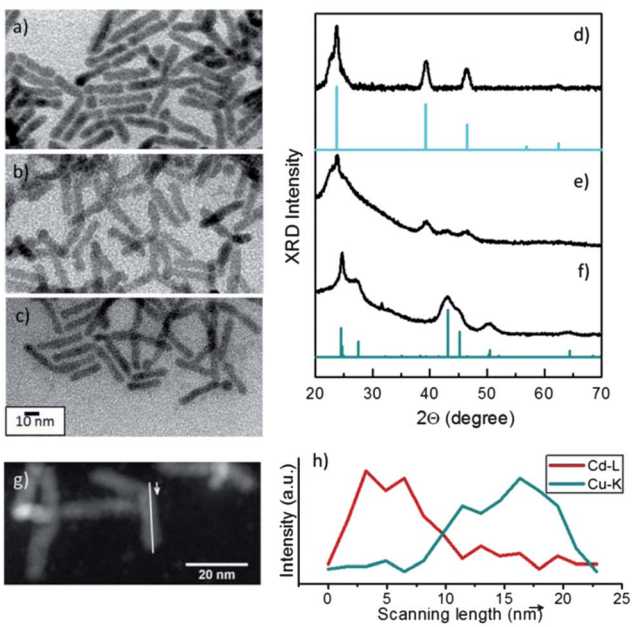

Fig. 1 (a–c) TEM images, and (d–f) corresponding XRD patterns of pure CdTe NRs (a and d), CdTe–$Cu_{2-x}Te$ heterostructures obtained upon partial cation exchange (b and e) and $Cu_{2-x}Te$ NRs resulting from complete cation exchange (c and f). The reference stick pattern in (d) corresponds to bulk CdTe with zincblende structure and in (f), to bulk $Cu_{2-x}Te$ with weissite crystal structure. (g) STEM image of a partially exchanged CdTe–$Cu_{2-x}Te$ nanorod sample. (h) Intensity of the Cd-L edge (red curve) and the Cu-K edge (blue curve) of a scan along a single CdTe–$Cu_{2-x}Te$ nanorod as indicated by the white arrow in (g).

The initial CdTe NRs are assigned to bulk CdTe with zincblende structure as determined *via* XRD (Fig. 1d). The XRD patterns of partially and fully exchanged NRs are shown in Fig. 1e and f, respectively. The XRD pattern of the completely exchanged nanorods is assigned to the weissite crystal structure of $Cu_{2-x}Te$ (Fig. 1f), as recently reported by us.[57] The XRD pattern of the partially exchanged nanorods (Fig. 1e) clearly shows a contribution of both, the initial CdTe zincblende and the final $Cu_{2-x}Te$ weissite crystal structures. This analysis indicates that the partially exchanged sample is composed in part of remaining CdTe and cation exchanged $Cu_{2-x}Te$. To confirm this we performed scanning transmission electron microscopy (STEM) measurements. With this technique it is possible to scan a single nanorod with a focused electron beam and collect the emitted X-rays, performing strongly localized energy dispersive X-ray analysis (EDX). Sensitive to the transitions occurring in the core electrons, this technique allows the determination of a distribution of elements along the structure. Representative data are shown in Fig. 1g and h. An EDX line profile (Fig. 1h) along one of the NRs (see white line in the STEM image (Fig. 1g)) indicates that cation exchange occurs in this NR preferentially from one side, yielding a clearly heterostructured CdTe–$Cu_{2-x}Te$ NR with a *ca.* 1 : 1 length ratio of both semiconductors. We would like to note here that even though in most NRs cation exchange starts from one of the NRs' tips, as shown in Fig. 1g and h, in some other NRs cation exchange starts simultaneously from both tips. We have also observed that in some of the CdTe–$Cu_{2-x}Te$ NRs analysed, not all Cd^{2+} ions could be completely removed (despite thorough sample washing), in turn leading to altered EDX spectra. We have also noted that upon electron beam exposure for HRTEM imaging, the $Cu_{2-x}Te$ sub-units degrade, *i.e.*, their crystal phase gets destroyed (Fig. S1,† ESI). Nevertheless, taken altogether, our results indicate that well-defined CdTe–$Cu_{2-x}Te$ NRs can be obtained upon partial cation exchange.

A typical absorption spectrum of the starting CdTe NRs is given in Fig. 2a. The spectrum is dominated by a sharp excitonic peak at 689 nm that reflects the quantum confinement of the CdTe NRs, the width of which is in the range of the exciton Bohr radius (~7.3 nm) in bulk CdTe.[52,73] Fig. 2b–e show the spectra of four batches of partially exchanged (CdTe–$Cu_{2-x}Te$) heterostructured nanorods. To denote the increasing contribution of the $Cu_{2-x}Te$ component in the CdTe–$Cu_{2-x}Te$ heterostructures from Fig. 2b to e, we indicate in the corresponding insets the volume of the Cu^+ stock solution added. All four spectra are characterized by an excitonic peak at *ca.* 689 nm. For CdTe–$Cu_{2-x}Te$ nanorods with a smaller portion of $Cu_{2-x}Te$ (*i.e.*, with a smaller amount of Cu^+ added, Fig. 2b and c) the excitonic peak from the CdTe sub-unit is clearly defined. However, with increasing amounts of Cu^+ added the contribution of the excitonic peak becomes gradually less apparent at the same time that the NIR plasmon band (arising from the increasing $Cu_{2-x}Te$ sub-unit) starts to dominate the spectral behaviour of the CdTe–$Cu_{2-x}Te$ heterostructures (Fig. 2d and e). After full exchange (Fig. 2f) the excitonic peak is completely suppressed and replaced by the typical absorption spectrum of pure $Cu_{2-x}Te$ NRs, dominated by a featureless absorption in the visible region and a strong plasmon resonance in the NIR region.[57,58] The above results are interpreted as follows. In the CdTe–$Cu_{2-x}Te$ heterostructures the excitonic peak at *ca.* 689 nm is present due to the remaining CdTe sub-unit, which becomes smaller with an increasing exchange of Cd^{2+} by Cu^+ ions (from Fig. 2b to e). On the other hand, the stronger contribution of the NIR resonance indicates an increasing $Cu_{2-x}Te$ part in the heterostructure.[58,61]

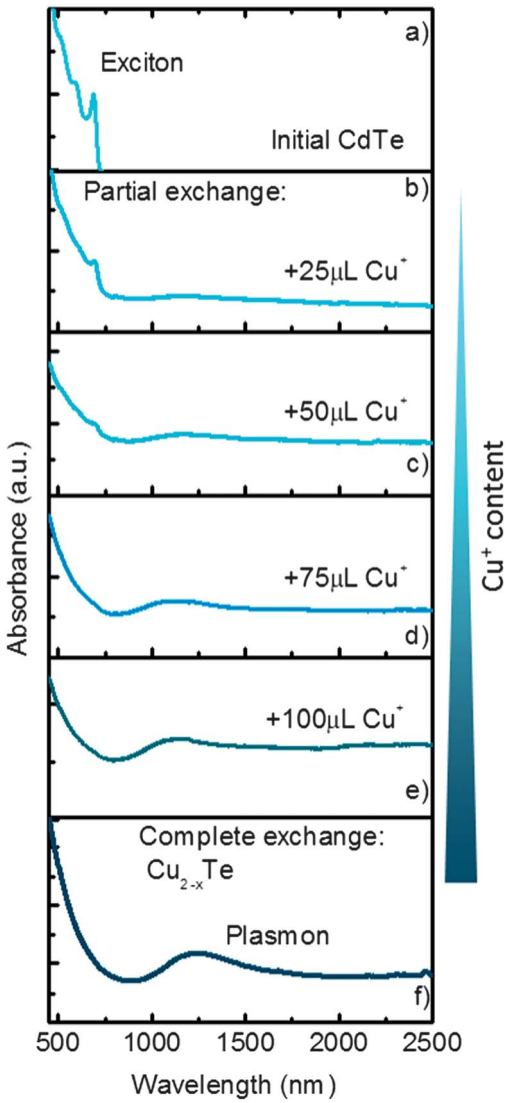

Fig. 2 Absorption spectra of (a) the initial CdTe NR sample; (b–e) CdTe–$Cu_{2-x}Te$ heterostructured NRs obtained upon partial cation exchange (the amount of Cu^+ added, and thus, the contribution of the $Cu_{2-x}Te$ sub-unit increases from (b) to (e)); and (f) the completely exchanged $Cu_{2-x}Te$ NRs. All spectra were measured in tetrachloroethylene.

So far we have shown that a partial exchange of Cd^{2+} by Cu^+ in the CdTe NRs results in CdTe–$Cu_{2-x}Te$ heterostructures, whose optical properties are dominated by the optical characteristics of the single components. A precise regulation of each contribution in the heterostructure is obtained by controlling the amount of Cu^+ added, and is attested by their respective

spectral signatures, namely the excitonic and plasmonic resonances. Now the question arises on how the systematic exchange of CdTe by $Cu_{2-x}Te$ affects the optoelectronic response of the CdTe–$Cu_{2-x}Te$ heterostructures. As a starting point we thoroughly analyzed the steady state absorption spectra in the exciton and plasmon resonance regions. Indeed, slightly broadened excitonic resonances can be distinguished along with the introduction of the $Cu_{2-x}Te$ component. We assign this broadening to an increased background absorption in that spectral region originating from the overlapping interband transitions of $Cu_{2-x}Te$ (see Fig. S2† in the ESI). Furthermore, any observed shift of the excitonic or plasmon resonances in the heterostructures (see Fig. S3† in the ESI) might be explained by an altered surface chemistry after the cation exchange process due to the supplementary addition of surface ligands (namely oleylamine, see Experimental section for details) to preserve colloidal stability during the process.[74–78] This altered surface chemistry might give rise to changes in the charge carrier density of the vacancy-doped sub-unit, and in turn result in a slightly modified optical response. This is particularly apparent in the localized surface plasmon resonance (Fig. S3c,† ESI).[79] We also remark here that upon partial cation exchange the photoluminescence (PL) from the CdTe sub-units in the CdTe–$Cu_{2-x}Te$ NRs gets significantly quenched and blue-shifts (Fig. S4,† ESI). These changes in PL cannot be solely ascribed to the presence of the newly formed plasmonic ($Cu_{2-x}Te$) sub-unit, but also to changes in the surface chemistry of the NRs occurring upon cation exchange. The impossibility to separate both effects makes it difficult to evaluate the effect of the plasmonic $Cu_{2-x}Te$ sub-unit on the PL of the excitonic CdTe one. This is the reason why we have mainly focused on the analysis of the steady state absorption spectra of the heterostructures.

A way to analyze the mutual influence of the CdTe exciton and the $Cu_{2-x}Te$ plasmon resonance in the heterostructures regardless of surface coverage is through optical modelling. As the plasmon resonance is generally described by electrodynamic theories as collective oscillations of the electron cloud,[80,81] we used the DDA (discrete dipole approximation)[82–84],§ to uncover electrodynamic effects that manipulate the optical response of the heterostructures. Note however that this model does not take into account an electronic 'contact' between the two materials, but treats the combined structure as if an infinite potential barrier were present at the hetero-interface. Nevertheless this approach leads to a reasonably good description of the steady state absorption of the combined system. The modelling of the heterostructures was performed by calculating the optical spectra of a single CdTe–$Cu_{2-x}Te$ nanorod hybrid with a variable length of the $Cu_{2-x}Te$ sub-unit and a fixed total length. The DDA method solves Maxwell's equations incorporating local dielectric functions of the nanorod sub-units. To model the $Cu_{2-x}Te$ part we used an empirical dielectric function of bulk $Cu_{2-x}Te$.[85] Note that in a previous study we have shown that with this dielectric function the NIR absorption properties of vacancy-doped copper telluride NCs of various shapes can be modelled and are in good agreement with the experimental results.[57] For the CdTe sub-unit, we used the following dielectric constant: $\varepsilon_{CdTe} = \varepsilon_{1,bulk} + i\delta\varepsilon_2$, where the real part $\varepsilon_{1,bulk}$ corresponds to bulk CdTe and is taken from the Palik tables,[86] and the imaginary part $\delta\varepsilon_2$ was extracted from fitting the calculated absorption to the experimental data for CdTe nanorods from Fig. 2a. The calculated spectra of the CdTe nanorods very closely reproduce the experimental ones. Thus, this approach allows us to describe empirically the size-quantization of excitons in CdTe nanorods. Fig. 3a (blue curve) displays the calculated absorption spectrum of a CdTe–$Cu_{2-x}Te$ nanorod of 21 × 5 nm (length × width). The heterostructured nanorod consists of two cylindrical segments of CdTe and $Cu_{2-x}Te$ equally sized (length × width = 10.5 × 5 nm). For simplicity, both segments will be termed "half rods" hereafter. Their absorption spectra are shown as solid (CdTe half rod) and dashed ($Cu_{2-x}Te$ half rod) black curves in Fig. 3a. The CdTe half rod shows a strong excitonic peak at 685 nm,

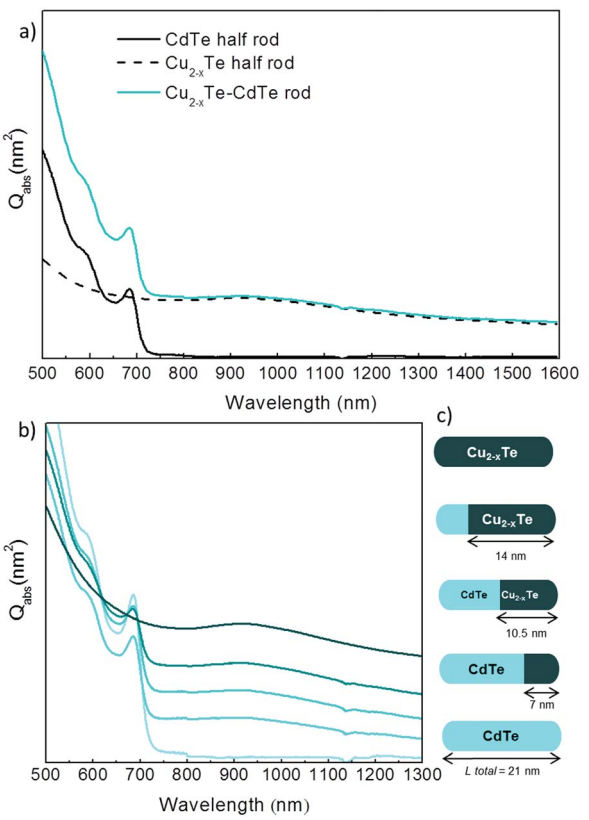

Fig. 3 (a) Calculated (DDA modelling) absorption spectra of a CdTe (black solid curve) and of a $Cu_{2-x}Te$ (black dashed curve) half rod (10.5 × 5 nm = length × width, see text for details). The spectrum in blue corresponds to a CdTe–$Cu_{2-x}Te$ heterostructured nanorod (21 × 5 nm) consisting of two CdTe and $Cu_{2-x}Te$ half rods with the above indicated dimensions. (b) Calculated absorption spectra (DDA) of CdTe–$Cu_{2-x}Te$ NRs with the following length ratios (upwards): $L_{CdTe} : L_{Cu_{2-x}Te}$ = 1 : 0, 2 : 1, 1 : 1, 1 : 2, 0 : 1. (c) Geometrical sketch (upwards) of the CdTe–$Cu_{2-x}Te$ NRs, whose spectra are depicted in (b).

§ The DDA code was taken from the open source at http://www.astro.princeton.edu/~draine/DDSCAT.html (accessed December 2012).

while the spectrum of the $Cu_{2-x}Te$ half rod is dominated by a broad plasmon resonance in the NIR centered at 935 nm. The spectrum of the heterostructured CdTe–$Cu_{2-x}Te$ nanorod results from the spectral addition of both half rods and as shown in Fig. 3a, both the excitonic and plasmonic contributions are well defined in the heterostructure, in agreement with the experimental results. Fig. 3b displays the calculated absorption spectra of CdTe–$Cu_{2-x}Te$ heterostructured nanorods (whose total length and width are 21 and 5 nm, respectively) having different length (L) fractions of each material. Specifically they have the following $L_{CdTe} : L_{Cu_{2-x}Te}$ length ratios (upwards): 1 : 0, 2 : 1, 1 : 1, 1 : 2 and 0 : 1 (see Fig. 3c). The results in Fig. 3b reproduce qualitatively the experimental spectra shown in Fig. 2b: depending on the length ratio of each material the intensity of the excitonic and plasmon peaks varies accordingly. Notably, the plasmon resonance in the heterostructured NRs remains rather unaffected by an increase in $Cu_{2-x}Te$ length-fraction (Fig. 3b and c, upwards), but also by the addition of the CdTe sub-unit. In a strongly plasmonic material one would expect a fundamental influence of the size,[87,88] but also of the refractive index of the surrounding medium.[89–92] CdTe has a refractive index much larger than the solvent or ligands surrounding the heterostructures. Therefore one would expect a strong red-shift of the plasmon resonance of $Cu_{2-x}Te$ upon contact with the CdTe sub-unit in the heterostructures. Both given findings indicate a weak plasmonic response of the $Cu_{2-x}Te$ moiety. This might be explained by carrier localization effects influencing the plasmonic response of the material, as recently reported by us.[57] Charge carriers in $Cu_{2-x}Te$ NCs, and in general in vacancy-doped copper chalcogenide NCs, show an essential degree of localization, *i.e.*, a Lorentz-like response.[57] This differs from the essentially free behaviour of electrons in plasmonic nanoparticles of noble metals (Drude-like), and in turn, results in a weaker plasmonic response in $Cu_{2-x}Te$. Remarkably, the calculated spectra qualitatively reproduce the experimental ones (note that any slight difference in the plasmon band position from sample to sample, see Fig. 2, may likely arise from slight differences in the degree of vacancy-doping of the $Cu_{2-x}Te$ moieties), and in fact they arise from the contribution of the individual sub-units (see Fig. 3a). This indicates a relatively weak ground state interaction between the optical excitations of the CdTe and $Cu_{2-x}Te$ sub-units. This weak ground state interaction might be explained by the low spectral overlap between the excitonic band of CdTe and the plasmonic resonance of $Cu_{2-x}Te$.[3] Furthermore, carrier localization effects in $Cu_{2-x}Te$ nanocrystals typically result in a low electric field enhancement, as recently shown,[57] which might in turn contribute to a weak interaction.

In any case, the presented optical modelling serves as a unique way to reproduce the absorption spectra of heterostructures with excitonic and plasmonic contributions, whilst neglecting any electronic interaction between the sub-units. An electronic interaction might for example result in broadening/weakening of the excitonic transitions or below gap absorption due to indirect transitions from the valence band of $Cu_{2-x}Te$ to the conduction band of CdTe. In our heterostructures, however, these features might be covered by the intense plasmonic signature from the $Cu_{2-x}Te$ sub-unit (Fig. S2,† ESI). A way to access the effect of such electronic interactions is pump-probe spectroscopy. In the following we will primarily set our focus on the excitonic response of the system. Despite the weak/negligible ground state interaction, it is expected that the addition of the $Cu_{2-x}Te$ sub-units largely influences the photoinduced process. We used pump-probe spectroscopy to investigate the charge carrier dynamics in the CdTe–$Cu_{2-x}Te$ heterostructures. We were particularly interested in the dynamics of the excitonic transition (arising from the CdTe) and its changes when increasing the size of the $Cu_{2-x}Te$ sub-unit, *i.e.*, with an increasing plasmonic contribution. Fig. 4a displays the measured transient spectra at different times ranging from 100 to 10 000 fs (from solid to broken curves) for a sample consisting of pure CdTe NRs (reference sample, top panel), and two CdTe–$Cu_{2-x}Te$ heterostructures with increasing plasmonic contribution (middle and bottom panels, respectively). In all cases the transient spectra at early times are dominated by bleach signals at ~690 nm, typically assigned to state-filling of the main excitonic transitions in a semiconductor NC.[93]

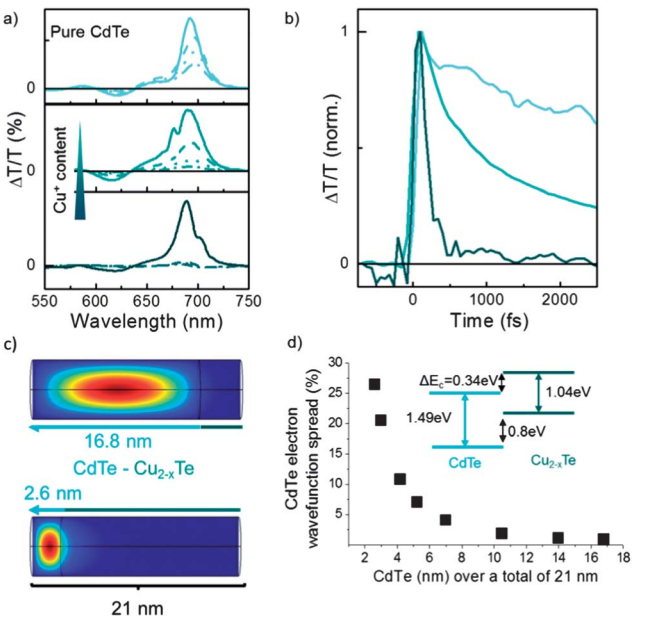

Fig. 4 (a) Transient absorption spectra of pure CdTe NRs (reference sample, top panel) and two CdTe–$Cu_{2-x}Te$ heterostructured NRs with increasing plasmonic contributions from the middle to the bottom panel. In all cases the time delay from the solid to broken curves is 0.1, 1, 4 and 10 ps. (b) Color-coded differential transmission dynamics for the three samples shown in (a) around the maximum bleach signal at ~690 nm (corresponding to the 1st excitonic transition at 689 nm). All curves are normalized at the maximum $\Delta T/T$ intensity. (c) False-colour representation of the electron wavefunction of the CdTe sub-unit from a CdTe–$Cu_{2-x}Te$ NR having a total length of 21 nm and a CdTe sub-unit length of 16.8 nm ($L_{CdTe} : L_{Cu_{2-x}Te} = 5 : 1$, top) and 2.6 nm ($L_{CdTe} : L_{Cu_{2-x}Te} = 1 : 7$, bottom). Note the electron wavefunction spread into the $Cu_{2-x}Te$ sub-unit in the heterostructure with a shorter CdTe. (d) CdTe electron wavefunction spread into the $Cu_{2-x}Te$ sub-unit as a function of the length of the CdTe sub-unit. The inset represents the CdTe–$Cu_{2-x}Te$ band alignment, as determined from ref. 72.

Additional photoinduced absorption (PA) signals are present due to a pump induced Stark shift of the electronic levels resulting from electric fields induced by localized carriers.[93,94] The main bleach signal corresponds to the 1st excitonic transition at 689 nm. While in the pure CdTe NR sample this signature is still strongly present within the first 10 ps (Fig. 4a, top panel), a faster decay is observed in the CdTe–$Cu_{2-x}Te$ heterostructures. The heterostructure with a smaller $Cu_{2-x}Te$ sub-unit (Fig. 4a, middle panel) shows a bleach signal that rapidly decays within the first 10 ps. In the heterostructure with a larger $Cu_{2-x}Te$ sub-unit (Fig. 4a, bottom panel) this signature has vanished within the first hundreds of femtoseconds. The dynamics at the maximum bleach signal for all three samples are given in Fig. 4b and clearly demonstrate that with increasing $Cu_{2-x}Te$ contribution the dynamics of the 1st excitonic transition are faster. We also remark here that the temperature of the lattice upon excitation increases by only tens of degrees.[95] In this regime, the diffusion of Cu^+ ions is not substantially activated. Furthermore, the lattice temperature returns to room temperature within 1 ms. Therefore, we do not expect a significant diffusion of Cu^+ ions into the CdTe sub-units during our pump-probe experiments.

In the following we try to discuss possible mechanisms that can affect the carrier dynamics in our system. Our CdTe–$Cu_{2-x}Te$ NRs are heterostructures with a type II band alignment[72] (see the inset in Fig. 4d), and thus their optoelectronic properties must be largely influenced by that, as thoroughly reported for other systems.[21–34] Upon photon absorption, the hole relaxes into the $Cu_{2-x}Te$ sub-unit, breaking the exciton and separating charges across the heterostructure. We assume, however, that the hole transfer from the CdTe sub-unit to the $Cu_{2-x}Te$ sub-unit cannot explain the observed enhanced decay of the $\Delta T/T$-signal (Fig. 4b) with increasing the size of the $Cu_{2-x}Te$ sub-unit. The reasons for that are two-fold. First, hole transfer is expected to be even faster than the observed decays.[93,96,97] Second, the holes are expected to contribute much less than the electrons to the bleaching signal of the CdTe exciton. Thus transferred holes cannot explain the pronounced and even complete recovery of the signal as observed in Fig.4a and b.

We now discuss that Auger recombination is probably responsible for the observed pump probe decay dynamics. In order to address this possibility we evaluated the degree of electron localization in the CdTe sub-unit through band structure calculations for heterostructures with different length-fractions (calculation details are given in the ESI†). The results for two heterostructures with different length-fractions, namely $L_{CdTe} : L_{Cu_{2-x}Te} = 1 : 7$ (top) and 5 : 1 (bottom), are depicted in Fig. 4c. While in both examples the electron is predominantly found in the CdTe sub-unit, it becomes clear that the shorter the CdTe sub-unit is, the more the electron wavefunction leaks into the $Cu_{2-x}Te$ sub-unit. Here, the high level of doping and carriers in the $Cu_{2-x}Te$ sub-unit might result in a greatly enhanced probability of Auger recombination. Indeed, in this process the energy resulting from electron–hole recombination is transferred to a third particle, namely an electron or a hole.[98] Thus, the Auger rate is here proportional to the hole carrier density. Moreover, since the overlap of the electron and hole wavefunctions is required for Auger recombination, the Auger rate increases proportionally to the spreading of the electron wavefunction in the $Cu_{2-x}Te$ sub-unit, and therefore increases with decreasing the length of the CdTe sub-unit. In Fig. 4d we plot the calculated fraction of the electron wavefunction spreading into the $Cu_{2-x}Te$ sub-unit as a function of the length of the CdTe sub-unit. We notice that with decreasing CdTe fraction from 10.5 to 3 nm the fraction of electron wavefunction spreading into the $Cu_{2-x}Te$ sub-unit increases by an order of magnitude ultimately facilitating Auger recombination pathways. This might explain: (i) the faster recombination dynamics in the heterostructures compared to the pure CdTe NRs (where the Auger recombination is presumably suppressed at the very low excitation densities used in the experiment) and (ii) the faster recombination dynamics in the heterostructured rods with shorter CdTe sub-units. However, we remark here that also energy transfer is conceivable to contribute to the decay dynamics in our heterostructures, despite the low spectral overlap between exciton and plasmon absorption. Indeed, such a non-resonant energy transfer to the surface plasmon of gold nanorods has been demonstrated to occur from dye molecules dispersed in the silica shell encapsulating the particles. In that case energy transfer occurs even though plasmon absorption lies in the absorption tail of the fluorophores.[99] Thus, the assignment of the faster dynamics to an Auger mediated or energy transfer mechanism in our CdTe–$Cu_{2-x}Te$ heterostructures is preliminary at this stage and these two photophysical scenarios will be thoroughly investigated in future work. However, we remark that energy transfer is expected to be much slower than the hole injection described above, and thus this favours our interpretation based on an Auger mediated recombination. In any case, our pump-probe data clearly indicate that the presence of an increasing plasmonic $Cu_{2-x}Te$ sub-unit in the heterostructures opens a faster decay channel for the CdTe exciton.

Conclusions

In this work we have demonstrated that cation exchange serves as a fast and efficient tool to design rod-shaped, type II, nano-heterostructures based on CdTe and $Cu_{2-x}Te$. We have shown that CdTe–$Cu_{2-x}Te$ NRs with sub-units of various length-fractions can be obtained by controlling the amount of the Cu^+ precursor added. Those heterostructures show an optical response with excitonic and plasmonic properties arising from the corresponding CdTe and $Cu_{2-x}Te$ sub-units. With DDA electrodynamic modelling of the nanorod absorption as originating from two independent sub-units, we were able to reproduce the excitonic and plasmonic peaks in the absorption spectra of the CdTe–$Cu_{2-x}Te$ NRs, despite their fundamentally different origin. The experimental and calculated absorption spectra of the heterostructures reveal a negligible ground state interaction between the CdTe exciton and the $Cu_{2-x}Te$ plasmon. This lack of a ground state interaction might result from the low spectral overlap between the excitonic transition in CdTe and the plasmon band in $Cu_{2-x}Te$. The weak size dependence and refractive index sensitivity of the $Cu_{2-x}Te$

plasmon resonance in the presence of the CdTe sub-unit might be explained by charge carrier localization effects in the $Cu_{2-x}Te$ sub-unit. These localization effects might in turn be responsible for the weak exciton–plasmon interaction. Nevertheless, we foresee important potential of cation exchange reactions to create semiconductor–semiconductor heterostructures with highly interacting excitons and plasmons through an appropriate choice of materials. For instance, the combination of PbSe and $Cu_{2-x}Se$ in a nanorod heterostructure might result in a larger spectral overlap and as such, in ground state exciton–plasmon interaction. Furthermore, ultrafast spectroscopy revealed a faster decay of the exciton in the presence of the $Cu_{2-x}Te$ sub-unit, and a faster decay the larger the plasmonic contribution from the $Cu_{2-x}Te$, *i.e.*, the larger the $Cu_{2-x}Te$ sub-unit gets. This faster dynamics may be due to an Auger mediated process, and hence we propose that for enhanced photovoltaic device performance a shorter Cu-based sub-unit is beneficial and that the suppression of carrier density within this sub-unit is of major importance. This delivers an important aspect with respect to the application of type II chalcogenide–chalcogenide heterostructures based on Cu and Cd for photovoltaic and photocatalytic applications.

Acknowledgements

J.F., J.R.F. and I.K. acknowledge the Bavarian Ministry of Science, Research and Arts for financial support through the project SolTech. J.R.F. acknowledges funding from the European Commission through the FP7-NMP programme (project UNION, grant agreement no. 310250). She also acknowledges funding from the LMUexcellent Junior Researcher Fund (project HE-Go-3D), within the DFG-funded Excellence Initiative. I.K. and F.S. acknowledge Fondazione Cariplo through the project EDONHIST (Grant no. 2012-0844). H.Z. and A.O.G. were supported by the U.S. Army Research Office under grant number W911NF-12-1-0407 and by Volkswagen Foundation (Germany). The use of the Center for Nanoscale Materials by A.O.G. and H.Z. was supported by the U. S. Department of Energy, Office of Science, Office of Basic Energy Sciences, under Contract No. DE-AC02-06CH11357.

References

1 R. Costi, A. E. Saunders and U. Banin, *Angew. Chem., Int. Ed.*, 2010, **49**, 4878–4897.
2 A. Vaneski, A. S. Susha, J. Rodríguez-Fernández, M. Berr, F. Jäckel, J. Feldmann and A. L. Rogach, *Adv. Funct. Mater.*, 2011, **21**, 1547–1556.
3 E. Shaviv, O. Schubert, M. Alves-Santos, G. Goldoni, R. Di Felice, F. Vallée, N. Del Fatti, U. Banin and C. Sönnichsen, *ACS Nano*, 2011, **5**, 4712–4719.
4 T. Mokari, E. Rothenberg, I. Popov, R. Costi and U. Banin, *Science*, 2004, **304**, 1787–1790.
5 T. Mokari, C. G. Sztrum, A. Salant, E. Rabani and U. Banin, *Nat. Mater.*, 2005, **4**, 855–863.
6 A. E. Saunders, I. Popov and U. Banin, *J. Phys. Chem. B*, 2006, **110**, 25421–25429.
7 L. Carbone and P. D. Cozzoli, *Nano Today*, 2010, **5**, 449–493.
8 G. Menagen, J. E. Macdonald, Y. Shemesh, I. Popov and U. Banin, *J. Am. Chem. Soc.*, 2009, **131**, 17406–17411.
9 G. Menagen, D. Mocatta, A. Salant, I. Popov, D. Dorfs and U. Banin, *Chem. Mater.*, 2008, **20**, 6900–6902.
10 M. J. Berr, F. F. Schweinberger, M. Döblinger, K. E. Sanwald, C. Wolff, J. Breimeier, A. S. Crampton, C. J. Ridge, M. Tschurl, U. Heiz, F. Jäckel and J. Feldmann, *Nano Lett.*, 2012, **12**, 5903–5906.
11 M. J. Berr, A. Vaneski, C. Mauser, S. Fischbach, A. S. Susha, A. L. Rogach, F. Jäckel and J. Feldmann, *Small*, 2012, **8**, 291–297.
12 M. Berr, A. Vaneski, A. S. Susha, J. Rodríguez-Fernández, M. Döblinger, F. Jäckel, A. L. Rogach and J. Feldmann, *Appl. Phys. Lett.*, 2010, **97**, 093108.
13 G. Dukovic, M. G. Merkle, J. H. Nelson, S. M. Hughes and A. P. Alivisatos, *Adv. Mater.*, 2008, **20**, 4306–4311.
14 J. Zhao, M. A. Holmes and F. E. Osterloh, *ACS Nano*, 2013, **7**, 4316–4325.
15 D. Mongin, E. Shaviv, P. Maioli, A. Crut, U. Banin, N. Del Fatti and F. Vallée, *ACS Nano*, 2012, **6**, 7034–7043.
16 M. B. Wilker, K. J. Schnitzenbaumer and G. Dukovic, *Isr. J. Chem.*, 2012, **52**, 1002–1015.
17 J. Lee, A. O. Govorov, J. Dulka and N. A. Kotov, *Nano Lett.*, 2004, **4**, 2323–2330.
18 G. P. Wiederrecht, G. A. Wurtz and J. Hranisavljevic, *Nano Lett.*, 2004, **4**, 2121–2125.
19 W. Zhang, A. O. Govorov and G. W. Bryant, *Phys. Rev. Lett.*, 2006, **97**, 146804.
20 N. T. Fofang, T.-H. Park, O. Neumann, N. A. Mirin, P. Nordlander and N. J. Halas, *Nano Lett.*, 2008, **8**, 3481–3487.
21 A. L. Rogach, T. A. Klar, J. M. Lupton, A. Meijerink and J. Feldmann, *J. Mater. Chem.*, 2009, 19.
22 C. Mauser, T. Limmer, E. Da Como, K. Becker, A. L. Rogach, J. Feldmann and D. V. Talapin, *Phys. Rev. B: Condens. Matter Mater. Phys.*, 2008, **77**, 153303.
23 J. Müller, J. M. Lupton, P. G. Lagoudakis, F. Schindler, R. Koeppe, A. L. Rogach, J. Feldmann, D. V. Talapin and H. Weller, *Nano Lett.*, 2005, **5**, 2044–2049.
24 J. Müller, J. M. Lupton, A. L. Rogach, J. Feldmann, D. V. Talapin and H. Weller, *Phys. Rev. B: Condens. Matter Mater. Phys.*, 2005, **72**, 205339.
25 D. V. Talapin, R. Koeppe, S. Gotzinger, A. Kornowski, J. M. Lupton, A. L. Rogach, O. Benson, J. Feldmann and H. Weller, *Nano Lett.*, 2003, **3**, 1677–1681.
26 M. Grazia Lupo, F. Scotognella, M. Zavelani-Rossi, G. Lanzani, L. Manna and F. Tassone, *Phys. Chem. Chem. Phys.*, 2012, **14**, 7420–7426.
27 M. Zavelani-Rossi, R. Krahne, G. Della Valle, S. Longhi, I. R. Franchini, S. Girardo, F. Scotognella, D. Pisignano, L. Manna, G. Lanzani and F. Tassone, *Laser Photonics Rev.*, 2012, **6**, 678–683.
28 F. Scotognella, K. Miszta, D. Dorfs, M. Zavelani-Rossi, R. Brescia, S. Marras, L. Manna, G. Lanzani and F. Tassone, *J. Phys. Chem. C*, 2011, **115**, 9005–9011.

29 M. R. Antognazza, F. Scotognella, K. Miszta, D. Dorfs, M. Zanella, M. Zavelani-Rossi, L. Manna, G. Lanzani and F. Tassone, *Phys. Chem. Chem. Phys.*, 2011, **13**, 15326–15330.

30 B. N. Pal, Y. Ghosh, S. Brovelli, R. Laocharoensuk, V. I. Klimov, J. A. Hollingsworth and H. Htoon, *Nano Lett.*, 2011, **12**, 331–336.

31 B. O. Dabbousi, J. Rodríguez-Viejo, F. V. Mikulec, J. R. Heine, H. Mattoussi, R. Ober, K. F. Jensen and M. G. Bawendi, *J. Phys. Chem. B*, 1997, **101**, 9463–9475.

32 S. A. Ivanov, J. Nanda, A. Piryatinski, M. Achermann, L. P. Balet, I. V. Bezel, P. O. Anikeeva, S. Tretiak and V. I. Klimov, *J. Phys. Chem. B*, 2004, **108**, 10625–10630.

33 S. Kumar, M. Jones, S. S. Lo and G. D. Scholes, *Small*, 2007, **3**, 1633–1639.

34 S. Kudera, L. Carbone, M. F. Casula, R. Cingolani, A. Falqui, E. Snoeck, W. J. Parak and L. Manna, *Nano Lett.*, 2005, **5**, 445–449.

35 M. A. Hines and P. Guyot-Sionnest, *J. Phys. Chem.*, 1996, **100**, 468–471.

36 D. Steiner, D. Dorfs, U. Banin, F. Della Sala, L. Manna and O. Millo, *Nano Lett.*, 2008, **8**, 2954–2958.

37 T. Teranishi and M. Sakamoto, *J. Phys. Chem. Lett.*, 2013, **4**, 2867–2873.

38 J. B. Rivest, S. L. Swisher, L.-K. Fong, H. Zheng and A. P. Alivisatos, *ACS Nano*, 2011, **5**, 3811–3816.

39 T. Teranishi, D. Inui, T. Yoshinaga, M. Saruyama, M. Kanehara, M. Sakamoto and A. Furube, *J. Mater. Chem. C*, 2013, **1**, 3391–3394.

40 X. Peng, M. C. Schlamp, A. V. Kadavanich and A. P. Alivisatos, *J. Am. Chem. Soc.*, 1997, **119**, 7019–7029.

41 L. Manna, E. C. Scher, L.-S. Li and A. P. Alivisatos, *J. Am. Chem. Soc.*, 2002, **124**, 7136–7145.

42 J. B. Rivest and P. K. Jain, *Chem. Soc. Rev.*, 2013, **42**, 89–96.

43 H. Li, R. Brescia, R. Krahne, G. Bertoni, M. J. P. Alcocer, C. D'Andrea, F. Scotognella, F. Tassone, M. Zanella, M. De Giorgi and L. Manna, *ACS Nano*, 2012, **6**, 1637–1647.

44 H. Li, M. Zanella, A. Genovese, M. Povia, A. Falqui, C. Giannini and L. Manna, *Nano Lett.*, 2011, **11**, 4964–4970.

45 K. Miszta, D. Dorfs, A. Genovese, M. R. Kim and L. Manna, *ACS Nano*, 2011, **5**, 7176–7183.

46 P. K. Jain, L. Amirav, S. Aloni and A. P. Alivisatos, *J. Am. Chem. Soc.*, 2010, **132**, 9997–9999.

47 S. Deka, K. Miszta, D. Dorfs, A. Genovese, G. Bertoni and L. Manna, *Nano Lett.*, 2010, **10**, 3770–3776.

48 B. Sadtler, D. O. Demchenko, H. Zheng, S. M. Hughes, M. G. Merkle, U. Dahmen, L.-W. Wang and A. P. Alivisatos, *J. Am. Chem. Soc.*, 2009, **131**, 5285–5293.

49 D. H. Son, S. M. Hughes, Y. Yin and A. Paul Alivisatos, *Science*, 2004, **306**, 1009–1012.

50 B. J. Beberwyck, Y. Surendranath and A. P. Alivisatos, *J. Phys. Chem. C*, 2013, **117**, 19759–19770.

51 R. D. Robinson, B. Sadtler, D. O. Demchenko, C. K. Erdonmez, L.-W. Wang and A. P. Alivisatos, *Science*, 2007, **317**, 355–358.

52 V. Esch, B. Fluegel, G. Khitrova, H. M. Gibbs, J. Xu, K. Kang, S. W. Koch, L. C. Liu, S. H. Risbud and N. Peyghambarian, *Phys. Rev. B: Condens. Matter Mater. Phys.*, 1990, **42**, 7450–7453.

53 A. L. Efros, M. Rosen, M. Kuno, M. Nirmal, D. J. Norris and M. Bawendi, *Phys. Rev. B: Condens. Matter Mater. Phys.*, 1996, **54**, 4843–4856.

54 M. G. Bawendi, M. L. Steigerwald and L. E. Brus, *Annu. Rev. Phys. Chem.*, 1990, **41**, 477–496.

55 P. Paufler, *Cryst. Res. Technol.*, 1988, **23**, 1360.

56 A. L. Efros and M. Rosen, *Annu. Rev. Mater. Sci.*, 2000, **30**, 475–521.

57 I. Kriegel, J. Rodríguez-Fernández, A. Wisnet, H. Zhang, C. Waurisch, A. Eychmüller, A. Dubavik, A. O. Govorov and J. Feldmann, *ACS Nano*, 2013, **7**, 4367–4377.

58 I. Kriegel, C. Jiang, J. Rodríguez-Fernández, R. D. Schaller, D. V. Talapin, E. da Como and J. Feldmann, *J. Am. Chem. Soc.*, 2012, **134**, 1583–1590.

59 W. Li, R. Zamani, P. Rivera Gil, B. Pelaz, M. Ibáñez, D. Cadavid, A. Shavel, R. A. Alvarez-Puebla, W. J. Parak, J. Arbiol and A. Cabot, *J. Am. Chem. Soc.*, 2013, **135**, 7098–7101.

60 A. L. Routzahn, S. L. White, L.-K. Fong and P. K. Jain, *Isr. J. Chem.*, 2012, **52**, 983–991.

61 J. M. Luther, P. K. Jain, T. Ewers and A. P. Alivisatos, *Nat. Mater.*, 2011, **10**, 361–366.

62 F. Scotognella, G. Valle, A. Srimath Kandada, M. Zavelani-Rossi, S. Longhi, G. Lanzani and F. Tassone, *Eur. Phys. J. B*, 2013, **86**, 1–13.

63 I. Kriegel, J. Rodríguez-Fernández, E. D. Como, A. A. Lutich, J. M. Szeifert and J. Feldmann, *Chem. Mater.*, 2011, **23**, 1830–1834.

64 S.-W. Hsu, W. Bryks and A. R. Tao, *Chem. Mater.*, 2012, **24**, 3765–3771.

65 S.-W. Hsu, K. On and A. R. Tao, *J. Am. Chem. Soc.*, 2011, **133**, 19072–19075.

66 Y. Xie, L. Carbone, C. Nobile, V. Grillo, S. D'Agostino, F. Della Sala, C. Giannini, D. Altamura, C. Oelsner, C. Kryschi and P. D. Cozzoli, *ACS Nano*, 2013, **7**, 7352–7369.

67 G. Della Valle, F. Scotognella, A. R. S. Kandada, M. Zavelani-Rossi, H. Li, M. Conforti, S. Longhi, L. Manna, G. Lanzani and F. Tassone, *J. Phys. Chem. Lett.*, 2013, 3337–3344.

68 F. Shieh, A. E. Saunders and B. A. Korgel, *J. Phys. Chem. B*, 2005, **109**, 8538–8542.

69 W. W. Yu, L. Qu, W. Guo and X. Peng, *Chem. Mater.*, 2003, **15**, 2854–2860.

70 D. Brida, C. Manzoni, G. Cirmi, D. Polli and G. Cerullo, *IEEE J. Sel. Top. Quant. Electron.*, 2012, **18**, 329–339.

71 A. I. Ekimov, F. Hache, M. C. Schanne-Klein, D. Ricard, C. Flytzanis, I. A. Kudryavtsev, T. V. Yazeva, A. V. Rodina and A. L. Efros, *J. Opt. Soc. Am. B*, 1993, **10**, 100–107.

72 B. Späth, K. Lakus-Wollny, J. Fritsche, C. S. Ferekides, A. Klein and W. Jaegermann, *Thin Solid Films*, 2007, **515**, 6172–6174.

73 W. W. Yu, Y. A. Wang and X. Peng, *Chem. Mater.*, 2003, **15**, 4300–4308.

74 B. P. Bloom, L.-B. Zhao, Y. Wang, D. H. Waldeck, R. Liu, P. Zhang and D. N. Beratan, *J. Phys. Chem. C*, 2013, **117**, 22401–22411.

75 M. T. Frederick, V. A. Amin and E. A. Weiss, *J. Phys. Chem. Lett.*, 2013, **4**, 634–640.

76 C. Bullen and P. Mulvaney, *Langmuir*, 2006, **22**, 3007–3013.

77 M. T. Frederick and E. A. Weiss, *ACS Nano*, 2010, **4**, 3195–3200.

78 M. T. Frederick, V. A. Amin, N. K. Swenson, A. Y. Ho and E. A. Weiss, *Nano Lett.*, 2012, **13**, 287–292.

79 X. Liu, X. Wang, B. Zhou, W.-C. Law, A. N. Cartwright and M. T. Swihart, *Adv. Funct. Mater.*, 2013, **23**, 1256–1264.

80 G. Mie, *Ann. Phys.*, 1908, **330**, 377–445.

81 U. Kreibig and M. Vollmer, *Optical Properties of Metal Clusters*, 1995.

82 B. T. Draine and P. J. Flatau, *J. Opt. Soc. Am. A*, 1994, **11**, 1491–1499.

83 P. J. Flatau and B. T. Draine, *Opt. Express*, 2012, **20**, 1247–1252.

84 B. T. Draine and P. J. Flatau, User Guide for the Discrete Dipole Approximation Code DDSCAT 7.2., http://arXiv.org/abs/1202.3424, Accessed December 2012.

85 B. S. Farag and S. A. Khodier, *Thin Solid Films*, 1991, **201**, 231–240.

86 E. D. Palik, *Handbook of Optical Constants of Solids*, Academic Press, New York, 1985.

87 J. Rodríguez-Fernández, J. Pérez-Juste, F. J. García de Abajo and L. M. Liz-Marzán, *Langmuir*, 2006, **22**, 7007–7010.

88 V. Myroshnychenko, J. Rodríguez-Fernández, I. Pastoriza-Santos, A. M. Funston, C. Novo, P. Mulvaney, L. M. Liz-Marzán and F. J. García de Abajo, *Chem. Soc. Rev.*, 2008, **37**, 1792–1805.

89 S. Underwood and P. Mulvaney, *Langmuir*, 1994, **10**, 3427–3430.

90 K. A. Willets and R. P. Van Duyne, *Annu. Rev. Phys. Chem.*, 2007, **58**, 267–297.

91 J. Rodríguez-Fernández, I. Pastoriza-Santos, J. Pérez-Juste, F. J. García de Abajo and L. M. Liz-Marzán, *J. Phys. Chem. C*, 2007, **111**, 13361–13366.

92 J. N. Anker, W. P. Hall, O. Lyandres, N. C. Shah, J. Zhao and R. P. Van Duyne, *Nat. Mater.*, 2008, **7**, 442–453.

93 V. I. Klimov, D. W. McBranch, C. A. Leatherdale and M. G. Bawendi, *Phys. Rev. B: Condens. Matter Mater. Phys.*, 1999, **60**, 13740–13749.

94 D. J. Norris, A. Sacra, C. B. Murray and M. G. Bawendi, *Phys. Rev. Lett.*, 1994, **72**, 2612–2615.

95 F. Scotognella, G. Della Valle, A. R. Srimath Kandada, D. Dorfs, M. Zavelani-Rossi, M. Conforti, K. Miszta, A. Comin, K. Korobchevskaya, G. Lanzani, L. Manna and F. Tassone, *Nano Lett.*, 2011, **11**, 4711–4717.

96 M. Saba, S. Minniberger, F. Quochi, J. Roither, M. Marceddu, A. Gocalinska, M. V. Kovalenko, D. V. Talapin, W. Heiss, A. Mura and G. Bongiovanni, *Adv. Mater.*, 2009, **21**, 4942–4946.

97 C.-H. Chuang, T. L. Doane, S. S. Lo, G. D. Scholes and C. Burda, *ACS Nano*, 2011, **5**, 6016–6024.

98 I. Robel, R. Gresback, U. Kortshagen, R. D. Schaller and V. I. Klimov, *Phys. Rev. Lett.*, 2009, **102**, 177404.

99 H. Su, Y. Zhong, T. Ming, J. Wang and K. S. Wong, *J. Phys. Chem. C*, 2012, **116**, 9259–9264.